
INTERPRETATION OF DEEP TEMPORAL REPRESENTATIONS BY SELECTIVE VISUALIZATION OF INTERNALLY ACTIVATED UNITS

A PREPRINT

Sohee Cho*

Graduate School of AI
KAIST
Daejeon, Republic of Korea
sohee.cho@kaist.ac.kr

Ginkyeng Lee*

School of Electrical and Computer Engineering
Ulsan National Institute of Science and Technology
Ulsan, Republic of Korea
gin908@unist.ac.kr

Jaesik Choi

Graduate School of AI
KAIST
Daejeon, Republic of Korea
jaesik.choi@kaist.ac.kr

April 28, 2020

ABSTRACT

Recently deep neural networks demonstrate competitive performances in classification and regression tasks for many temporal or sequential data. However, it is still hard to understand the classification mechanisms of temporal deep neural networks. In this paper, we propose two new frameworks to visualize temporal representations learned from deep neural networks. Given input data and output, our algorithm interprets the decision of temporal neural network by extracting highly activated periods and visualizes a sub-sequence of input data which contributes to activate the units. Furthermore, we characterize such sub-sequences with clustering and calculate the uncertainty of the suggested type and actual data. We also suggest Layer-wise Relevance from the output of a unit, not from the final output, with backward Monte-Carlo dropout to show the relevance scores of each input point to activate units with providing a visual representation of the uncertainty about this impact.

Keywords Time Series · Clustering · Input Attribution · Deep Convolutional Neural Network · Uncertainty

1 Introduction

The amount of temporal data is growing rapidly due to the inexpensive and diverse automatic-information systems such as manufacturing sensors, stock database systems, and healthcare wearable devices. Deep learning models extract appropriate features with a large amount of data and make decisions. As a result, there is growing demands to apply deep learning methods to such vast temporal data in various fields. However, users in areas that highly require transparency and accuracy of decision-making are still hesitant to use AI's decision due to the lack of interpretability of the internal process.

Recently many efforts have been made to interpret the decision process of deep learning models. Interpretable machine learning methods explain or interpret decisions of complex artificial intelligence systems with illustrative or textual descriptions. These approaches for deep learning are classified as explaining input attribution by relevance score based methods [1, 2, 3, 4] and gradient-based methods [5, 6, 7] explaining internal nodes [8, 9], explaining through attention [10, 11] and generating explanations [12].

*Both authors contributed equally to this research.

However, those methods are mainly used in the image domain, because visualized outputs with an input itself enables users to intuitively interpret what the outputs mean. In Network Dissection [8], for example, input images and the highlighted regions of outputs show what is the role of a specific unit. Layer-wise Relevance Propagation [2] explains the model’s decision by decomposing an output of the model into each input pixel by the amount of contributing to the output, so that people can visually separate complex elements such as shape and color. Applying those techniques to time series data, we consider the following challenges;

- While the result of input attribution is represented by a time point, it is difficult to find semi-global shapes of features.
- Input attribution methods only indicate which part effects on model’s decision without certainty. It is difficult to determine whether we certain it or not.

To solve these problems, we suggest two new frameworks to visualize temporal representations with the role of units of deep neural networks with uncertainty. Our methods suggest the following solutions for each problem.

- Instead of interpreting a whole learned network at once, we analyze the role of a unit in the trained network and find out which elements of an input have affected to activate units. First, we characterize the important sub-sequences of inputs to activate units. Second, we propose the extension of Layer-wise Relevance Propagation from the unit, not from the final output.
- We suggest to visualize quantified uncertainty. First, we represent the difference between the clustered pattern and the actual data. Second, we approximate the distributions of input relevance score to activate units using Monte-Carlo dropout through the backward part.

2 Related Work

Table 1: Comparison with XAI methods and proposed methods. *PBP stands for point by point.

	LRP	NETWORK DISSECTION	UNIT LRP	CPHAP
UNIT-SPECIFIC ANALYSIS	X	O	O	O
APPLICABILITY ON TIME SERIES	O	X	O	O
DESCRIPTION METHOD	PBP	SUB-INPUT	PBP	SUB-INPUT

2.1 Convolutional Neural Network (CNN)

Role of filter Convolutional Neural Network (CNN) [13] can be divided into two parts that extract the features of the input and classify the classes. Filters in CNN learn to extract various and appropriate features from input to reduce costs during the training procedure. The value of the feature map from the learned filter is the part that affects the final output through convolution.

Receptive field In a convolutional layer, the spatial region of the unit receives input from only a restricted subarea of the previous layer. The input area of that region is called its receptive field. Therefore, the deeper the layer is, the longer the receptive field of the input is mapped.

2.2 Layer-wise Relevance Propagation (LRP)

[2] proposes a 127 general solution to the problem of understanding classification decisions by pixel-wise decomposition of nonlinear classifiers using the Taylor decomposition. The idea is extended to deep neural networks by the divide-and-conquer paradigm, by exploiting the property that the function learned by a deep network is structurally decomposed into a set of simpler sub-functions that relate quantities in adjacent layers [14].

2.3 Network Dissection

Network Dissection [8] is a method for quantifying the interpretability of individual units in a deep CNN. This is a method for evaluating the degree of matching of a unit and corresponding concepts from a segmentation label of input

space. At this time, the match between a unit k and a concept c is quantified through the Intersection over Union score (IoU). Therefore, this approach is not applicable for dataset without segmentation labels such as most of the time series data.

2.4 Monte-Carlo Dropout as Bayesian Approximation

It has been shown that the use of dropout in neural networks can be interpreted as a Bayesian approximation of a Gaussian process, a well known probabilistic model [15]. This approach, called **Monte Carlo dropout**, mitigates the problem of representing model uncertainty in deep learning without sacrificing either computational complexity or test accuracy and can be used for all kinds of models trained with dropout. Modeling uncertainty with Monte Carlo dropout works by running multiple forward passes through the model with different dropout masks with probability p for every iteration.

2.5 Time Series Decomposition

To interpret time series, [16, 17] decompose an input time series into trend, seasonality, and holidays. The part of decomposed time series could interpret characteristics of time series through long-term tendency. However, such tendency differs from the shape of the input time series so that it is not enough to interpret the input time series itself.

3 Clustered Pattern of Highly Activated Period (CPHAP)

This section presents our algorithm that interprets the decision of temporal neural networks by extracting highly activated units and visualizes sub-sequences of input data which contributes to activating the units. Furthermore, we characterize such sub-sequences with clustering and calculate the uncertainty of suggested types and actual data.

- **Notion**
 - $T_{j,k}$: threshold
 - $a_{j,k}$: unit k at a hidden layer j , an activation map
 - i : a node of unit
- **Highly Activated Period (HAP):** *Highly Activated* means some nodes in an activation map have bigger values than a thresholds. We calculate a threshold $T_{j,k}$ satisfying equation 1 for each unit to selectively extract highly activated temporal period for unit $a_{j,k}$.

$$P(a_{j,k} > T_{j,k}) = 0.05. \quad (1)$$

Then, we define **HAP** as a set of nodes of activation map $a_{j,k}$ satisfying following equation.

$$\mathbf{HAP} = \{i \in [1, |a_{j,k}|] | a_{j,k}[i] > T_{j,k}\} \quad (2)$$

- **Trigger Input Sub-Sequence (TISS):** TISS is a set of input receptive fields of HAP.

$$\mathbf{TISS} = \{\text{Input receptive field}(i, j) | i \in \mathbf{HAP}\} \quad (3)$$

- **Pattern:** A pattern is a mean over a time axis of sub-cluster outputs.

$$\mathbf{Pattern} = \{p \in \text{subcluster} | \mu_{\text{subcluster}}\} \quad (4)$$

3.1 Patternize important Sub-Sequence of Input to Activate Unit by Clustering

In this section, we characterize the sub-sequences that play important roles in activating the unit by clustering. We suggest clustering in two stages; super-cluster and sub-cluster. A super-cluster describes the overall shape of the input sequences, e.g., decreasing shape. It shows a big trend in input sequences. On the contrary, a sub-cluster is divided according to the distribution of data in each super-cluster. For example, a sub-cluster of super-clusters that has declining shape could be sequences that are decreased step by step, or smoothly declining. That is, the shape of the input sequence can be checked through the super-cluster, and the detailed shape can be checked through the sub-cluster.

We employ the K-shape clustering [18] as a super-cluster and the Gaussian Mixture Models (GMMs) as a sub-cluster. When we divide results of a super cluster into sub-clusters, the number of a sub-cluster is determined by the number and the standard deviation of sub-sequences. Also, the sub-cluster with a standard deviation greater than 1.6 is ignored. Eventually, we call a mean of such sub-cluster as a pattern.

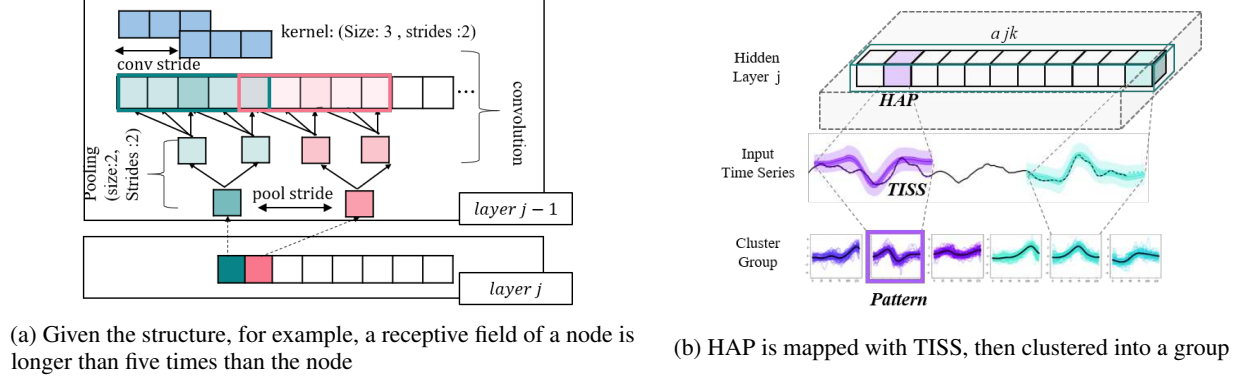


Figure 1: Overall process of CPHAP

Algorithm 1 Extract patterns from important input sub-sequence by clustering

Input: data \mathbf{X} , Super-cluster number s , Trained Convolution neural network $f_{1,\{c|c \in c_1\}} (f_{2,\{c|c \in c_2\}} (\dots f_{L,\{i|i \in c_L\}} (\cdot)))$
 $a_{j,k} = f_{1,\{c|c \in c_1\}} (f_{2,\{c|c \in c_2\}} (\dots f_{j,k} (\mathbf{X})))$
for k **do**
 $P(a_{j,k} > T_{j,k}) = 0.05$
 $\mathbf{HAP} = \{i \in [1, |a_{j,k}|] | a_{j,k}[i] > T_{j,k}\}$
 $\mathbf{TISS} = \{\text{Input receptive field}(i, j) | i \in \mathbf{HAP}\}$
end for
 $N_{sup} = \text{Set as having least B.I.C score}$
 $\mathbf{SUP}_p = \{x \in \mathbf{X} | K - \text{shape}(x) = p\}$
 $N_{sub} = \text{int}(\sqrt{\mu\text{std}(\mathbf{SUP}_p)} \times \sqrt{|\mathbf{SUP}_p|})$
 $\mathbf{SUB}_{p,b} = \{x \in \mathbf{SUP}_p | \text{GMM}(x, N_{sub}) = b\}$
DELETE $\mathbf{SUB}_{p,b}$ **if** $\text{std}(\mathbf{SUB}_{p,b}) > 1.6$
 $\mathbf{PATTERN}_{p,b} = \mu\mathbf{SUB}_{p,b}$
 $\mathbf{UNCERTAINTY}_{p,b} = P(\text{cluster}\{p, b\} | \mathbf{SUB}_{p,b})$

3.2 Uncertainty Analysis

The uncertainty in CPHAP is the average of entropy for the posterior probability of the corresponding the input sub-sequences and indicates how much certainty the input sequences belongs to a cluster. Input sub-sequences, that appear frequently in a set of the receptive field of the spatial region of the highly activated unit and have distinctive shapes, belongs to an less uncertainty of cluster. In contrast, sub-sequences, nor have characteristic shape neither appear on the main input, belongs into the rest cluster which have very large variance clusters.

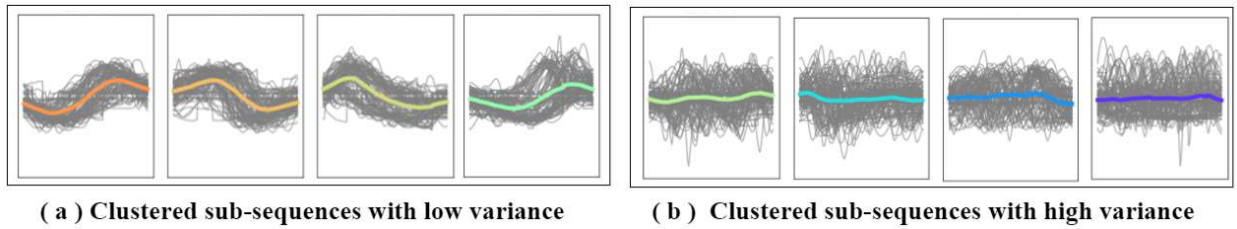


Figure 2: Clustered sub-sequence through k-means.(a) low variance with low uncertainty, (b)high variance with high uncertainty

4 Unit-Layer-wise Relevance Propagation with uncertainty

We also propose Layer-wise Relevance Propagation from the output of an internal unit, not from the final output. With the backward Monte-Carlo dropout, our algorithm also shows the relevance score of each input point to activate

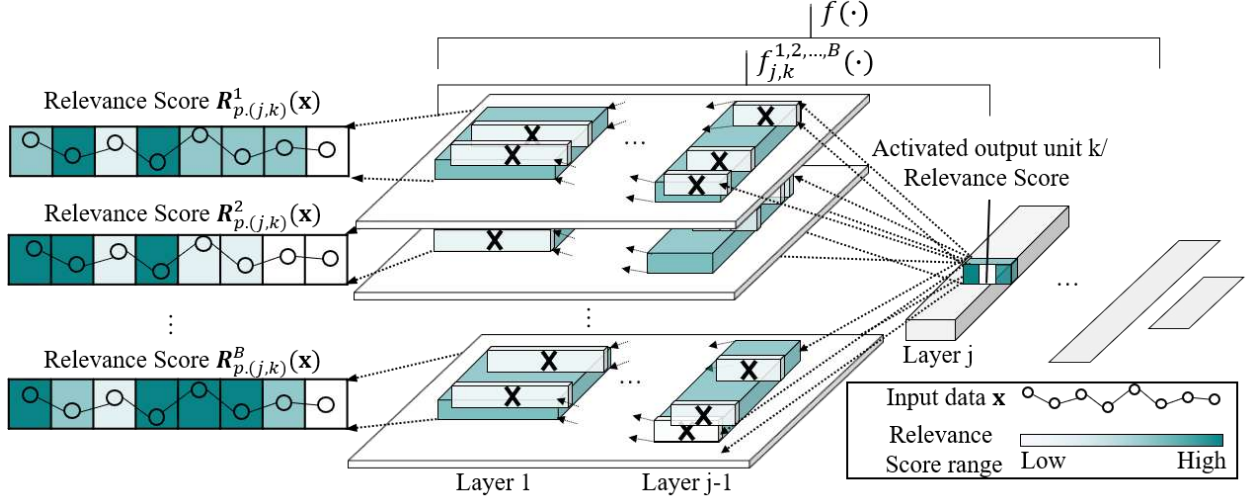


Figure 3: A description of Unit-Layer-wise Relevance Propagation from unit k at layer j with B backward Monte-Carlo dropout. We obtain B different random sampled input attributions for unit k . With these samples, we approximate the distribution of input attribution.

Algorithm 2 Input Attribution with Monte-Carlo dropout Network

Input: data \mathbf{X} , number of dropout iterations B , dropout probability dp , Trained Convolution neural network $f_{1,\{c|c \in c_1\}}(f_{2,\{c|c \in c_2\}}(\dots f_{L,\{i|i \in c_L\}}(\cdot)))$

$f_{j,k} = f_{1,\{c|c \in c_1\}}(f_{2,\{c|c \in c_2\}}(\dots f_{j,k}(\cdot)))$

for $b = 1$ **to** B **do**

$f_{j,k}^b = \text{Dropout}(f_{j,k}, dp)$

$\mathbf{R}_{p(j,k)}^b(\mathbf{X}) = \text{Taylor decomposition from unit } k \text{ to input with randomly sampled trained network } f_b^{j,k}$

end for

$\hat{\mathbf{R}}_{(p),j,k} = \frac{1}{B} \sum_{b=1}^B \mathbf{R}_{p(j,k)}^b$

$\text{Var}(\hat{\mathbf{R}}_{(p),j,k}) = \frac{1}{B} \sum_{b=1}^B [\hat{\mathbf{R}}_{(p),j,k} - \mathbf{R}_{(p),j,k}^b]^2$

units by providing the visual representation of the uncertainty about the relevance score. We call this method as **Unit-Layer-wise Relevance Propagation (Unit-LRP) with uncertainty**.

4.1 Unit-Layer-wise Relevance Propagation

We only consider $f_{j,k}$ which represents the part of a trained neural network from unit k at layer j , instead of the whole neural network f . It helps to understand how much the input affects to activate the unit k , not to final output. In other words, we try to the interpretation by the unit rather than the final output. The description in the aspect of the final output is hard to interpret especially for the time series data, because such description is a composite of the whole description of the various features.

We map a set of neurons x_i at i layer in $f_{j,k}$ to the relevance R_j which is the relevance of the next layer at the output direction. And we assign ((what?)) to a neuron x_j . Assuming that these two objects are functionally related by a function $R_j(x_i)$, we can apply Taylor decomposition on this local function in order to redistribute relevance R_j onto lower-layer relevance R_i . Running this redistribution procedure from unit k in the backward pass leads to the pixel-wise relevance $R_{p(j,k)}$ that forms the heatmap of the input attribution for unit activation. The input attribution obtained here represents the score of a positive influence on activating the unit.

4.2 Uncertainty Analysis

We extend beyond deterministic modeling using Monte-Carlo dropout with the backward passes with part of a trained network from input to the unit(((I can't understand))). We get random samples generated from the posterior predictive

distribution of relevance score for the part of the trained network $f_{j,k}^b$, $b = 1, \dots, B$. As a result, the uncertainty of input attributions can be estimated by the sample variance of multiple scores in a few repetitions.

This uncertainty represents how much the unit-LRP score can be agreed with the conventional model. Even if the input attribution is high but the uncertainty is low, we should look carefully at whether such input temporal point has a positive effect on the unit's activation. On the contrary, the temporal point of input with low input attribution and high uncertainty has a possibility of affecting the activation of the unit.

5 Experimental Result

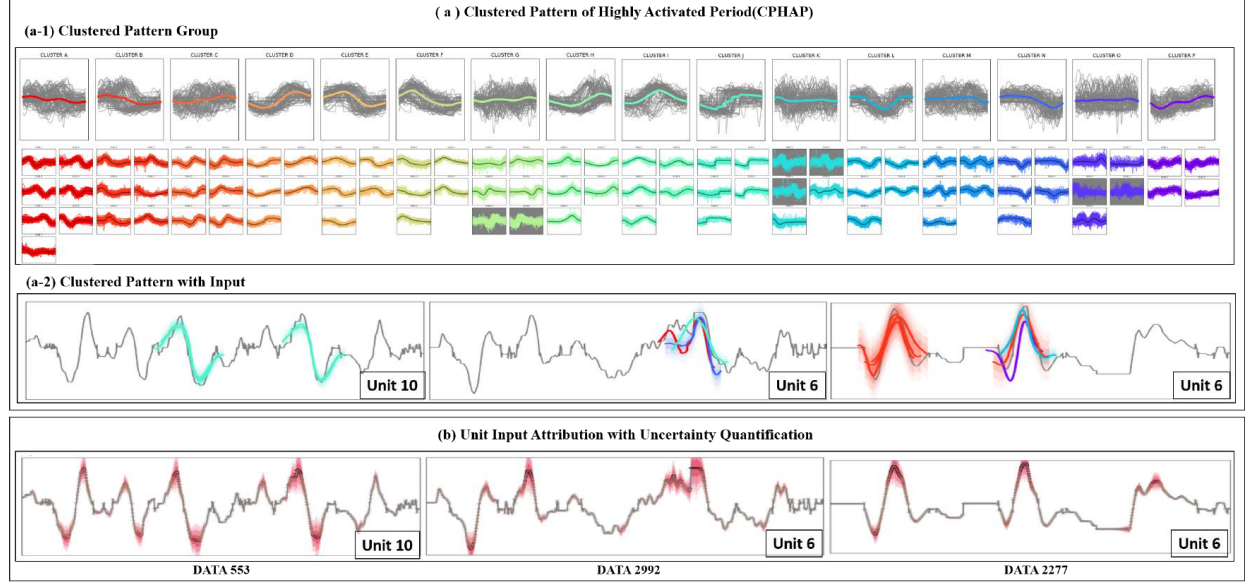


Figure 4: Visualizations of temporal representations learned from temporal deep neural networks when identifying the role of units for model determination by two proposed methods; (a) clustered pattern of highly activated period and (b) unit input attribution with uncertainty quantification. (a-1) are clustered pattern groups and (a-2) are inputs and input sub-sequences highly activating units with a color of clustered pattern group and shadow. The color means which cluster a sub-sequence belongs to and the shadow means how much uncertain the pattern is. (b) is unit input attribution with uncertainty quantification. The positive relevance score of the input to activate unit is shown as red for each time point. Darker red represents the larger relevance score. The uncertainty is represented by the area size of the red shadow at a specific time point.

Table 2: Dataset and description of model structures

DATA SET	TIME LENGTH	INPUT CHANNEL	CLASS	CNN ACCURACY	POOL1	CONV1	CONV2	POOL2	CONV3	POOL3
UWAVE	945	1	9	98.18%	15,2	8,4	11,2	8,4	7,2	4,2
HAR	128	9	6	79%	7,2	4,2	5,1	4,2	3,1	2,1
EEG	117	14	2	99%	7,2	4,2	5,1	4,2	3,1	2,1

Dataset We use three open time series dataset for experiments; *UWaveGestureLibraryAll* [19] is a set of eight simple gestures generated from accelerometers, *Smartphone Dataset for Human Activity Recognition (HAR)* [20] is a smartphone sensor dataset recording human perform eight different activities, and *Electroencephalography (EEG)* [21] is a sensor record that detects electrical activity in human brain while a human opens or closes eyes.

Model We use a temporal CNNs which is composed of three convolution layers followed by pooling layers, and one fully connected layer. ReLu function is used as the activation function in every hidden layer. Batch size and epoch are 64 and 500 respectively. In the prediction phase, we choice the model with the lowest validation loss.

Parameter for Algorithms For *Clustered Pattern Highly Activated Period* method, we use 16,16 and 12 clusters for super-cluster respectively. For *Unit-Layer-wise Relevance Propagation* method, we sample 300 times of Monte-Carlo Dropout with a rate for 0.5 before the non-linear activation function.

5.1 Clustering Methods

We compare several clustering methods to suggest the optimal algorithm for characterizing input sub-sequences with a measure of shape and distribution. We experimentally try to various methods; k-means, Gaussian Mixture Models (GMMs) and K-shape. The outputs of each method are in appendix figure 12, 13 14 .

K-means K-means classifies nearby sequences into the same cluster based on Euclidean distance only. Therefore, this method does not guarantee that sequences with the same shape but different positional information are clustered into the same group.

GMM GMMs assume that there are a certain number of Gaussian distributions, and each of these distributions represents a cluster. Therefore, it is not a suitable clustering method for our algorithm as it does not distinguish based on shape.

K-shape K-shape [18] is a similar with K-means, but specialized for time series, comparing the sequences efficiently and computing centroids effectively under the scaling and shift invariances. However, k-shape has a similar problems like k-means.

As these single clusters have some problems of not distinguishing each cluster or lack of detail, we combine two clustering methods sequentially.

GMM & K-shape When we use GMM first and then re-cluster each result of GMM to K-shape clustering, this combined clustering method considers both shape and distribution. However, since this clustering is based on data distribution first, the representative shape of each cluster does not sufficiently reflect the shapes of the sequences in the cluster.

K-shape & GMM When we use K-shape clustering first then re-cluster each result of K-shape clustering to GMM, this combined clustering method also considers both shape and distribution. Since this clustering is based on data shape first, the representative shape of each cluster is enough to characterize each group.

5.2 The role of the unit in CPHAP

To analyze the relationships between unit and class labels, we perform the following steps.

1. $freq_{U,P}$: Count patterns p contributing to activating units u for every u and p pair.
2. $freq_{P,C}$: Count patterns p belonging in the class c for every p and c pair.
3. $freq_{U,C}$: Multiply $freq_{U,P}$ and $freq_{P,C}$.

The value of $freq_{U,C}[u, c]$ indicates how much unit u pays attention to frequent pattern in class c .

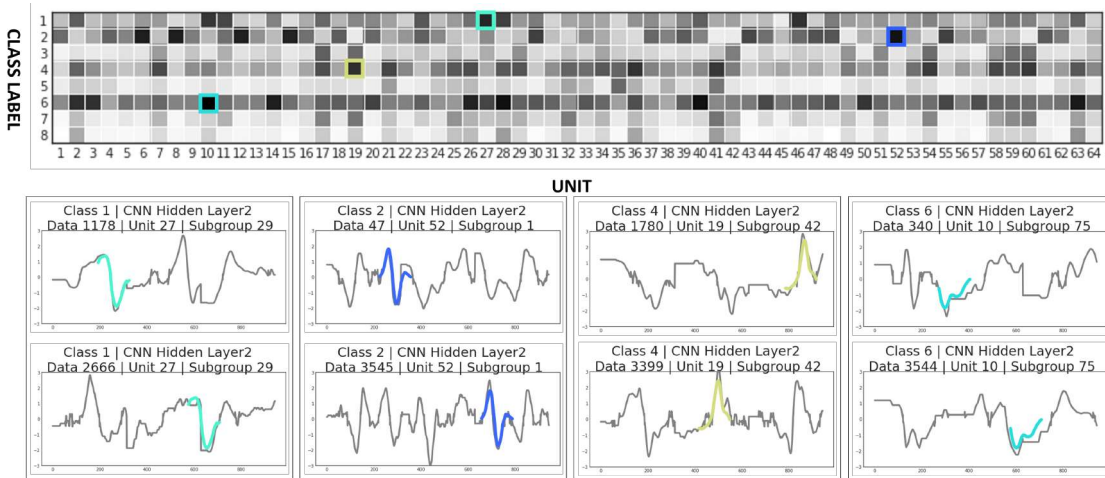


Figure 5: (Top) Highly related class-unit pairs are (Class1-Unit27) , (Class2-unit52), (Class4-unit19) and (Class6-unit10) in EEG Dataset. (Bottom) Visualization of the 4 most distinguishable Class-Unit relationships for Uwave with the color of the pattern that is mostly activated the corresponding unit.

Uwave Dataset Figure 5 is the frequency matrix $frequ_{u,c}$ from CNN, layer2 with Uwave dataset and it visualizes the 4 most distinguishable Class-Unit relationships with the color of the patterns that is mostly activated the corresponding unit. (Column 1) We can see the relationships with Class 1 and Unit 27 in layer2, CNN. Unit 27 is mainly activated by a sub-sequence similar to an inverted concave shape, frequently seen in class 1. (Column 2) Unit 52 is activated by the concave and convex patterns, so we can infer that this activation of unit 52 plays a major role to classify whether this input is class 2 or not. (Column 3) In Class 4 classification, the role of unit 19, which primarily looks like a convex shape, stands out. (Column 4) To predict class 6, unit 10 is activated by an alphabet 'W' shape.

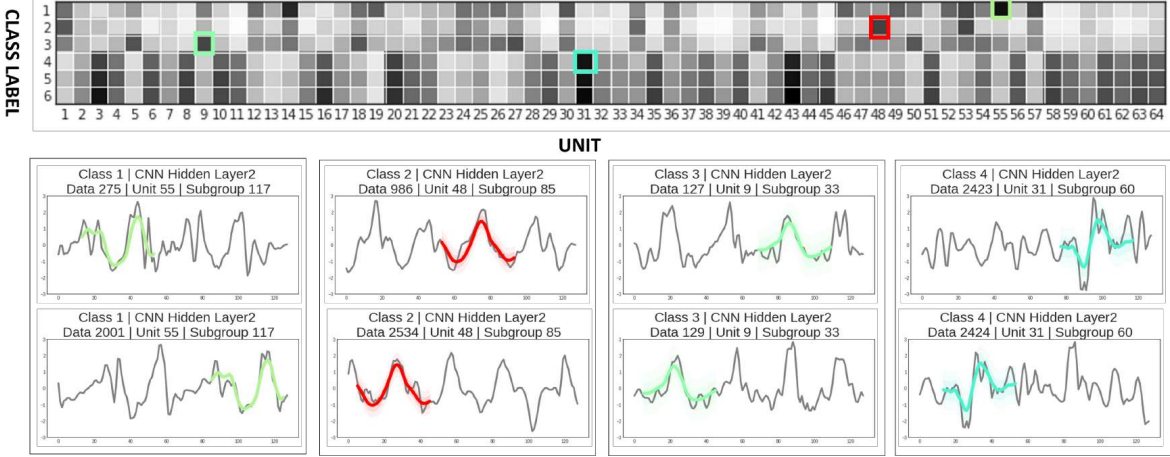


Figure 6: (Top) Highly related class-unit pairs are (Class1-Unit55) , (Class2-unit48), (Class3-unit9) and (Class4-unit31) in HAR Dataset. (Bottom) Visualization of the 3 most distinguishable Class-Unit relationships for HAR with the color of the pattern that is mostly activated in the corresponding unit.

HAR Dataset Figure 6 is the frequency matrix $frequ_{u,c}$ from CNN, layer2 for HAR dataset. (Column 1) In predicting class 1, unit 55 focuses on sub-cluster 7. This unit is activated by a combination of short convex and long concave shapes. (Column 2) Similarly, unit 48 plays an important role to predict class 2. This unit is mainly activated by the sub-cluster 85, which is represented in a red thick line. (Column 3) Unit 9 is relevant when estimating class 3. It is primarily activated by the pattern with shape of rapidly decreasing and increasing in the center. (Column 4) Also, Unit 31 finds the main features to predict class 4. This unit is primarily activated in bright blue-green patterns.

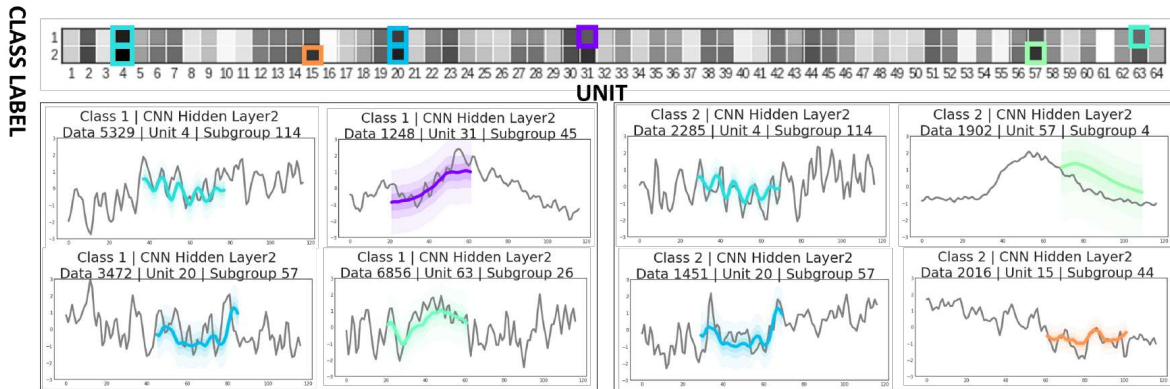


Figure 7: (Top) Highly related class-unit pairs are (Class 1,2-Unit 20, Unit 4), (Class 1-Unit 31, Unit 63), and (Class2-Unit 57, Unit 15) in EEG Dataset. (Bottom) Visualization of the common unit for Class 1,2 and specialized unit for each class 1 and 2 with the color of the pattern that is mostly activated the corresponding unit.

EEG Dataset Figure 7 indicates that highly activated units of two classes are almost same. However, several units for each class also play a specialized role because the model has trained to distinguish these two classes. (Column 1,3) Unit 4 of CNN, layer2 is activated by zigzag shape. This unit affects when predicting both Classes 1 and 2. Similarly, unit 20 is activated mainly by sub-clusters 57, which are represented by the W shape. (Column 2,4) On the other hand,

column 2,4 represent the role of more specialized units in each class. Column 2 shows the role of units 31 and 63 to classify class 1 and column 4 well shows the role of units 57 and 15 to classify class 2.

5.3 The role of the unit in Unit-LRP with uncertainty

This experiment shows how different **CPHAP** and **unit-LRP with uncertainty** represent the role of units to classify classes. **CPHAP** describes the role of an important unit with patterns corresponding to the input sub-sequences. On the other hand, **unit-LRP with uncertainty** provides the interpretability for decisions of the model through point-by-point of input rather than input sub-sequences. Figure 8,9,10 use the same data and unit so that they show differences between two proposed methods. The Unit-LRP score is represented by red color and the darker the red is, the higher the relevance score is. Contour with red color indicates the uncertainty of the corresponding relevance score. We analyze for each data below.

UWAVE Dataset Figure 8 is an output of Unit-LRP from CNN, layer2 for Uwave dataset. (Column 1) Unit 27 is mainly activated by peak points or the lowest points of each period. (Column 2) Similarly, Unit 52 is activated by both peaks or lowest points. (Column 3) Unit 19 is activated by the highest peak points and its red color is darker than others. (Column 4) Opposite column three, unit 10 is activated by the lowest point of each period. As contours are thicker than others, this unit has higher uncertainty than others.

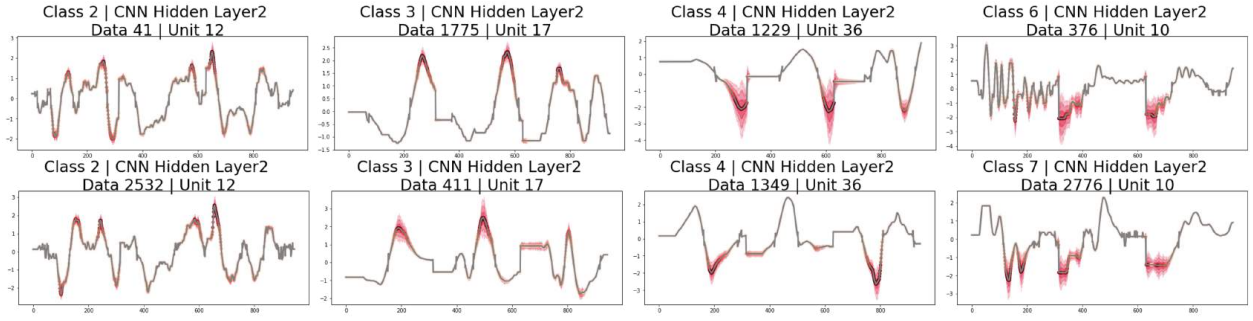


Figure 8: Unit-LRP with uncertainty result from Uwave dataset

HAR Dataset Figure 9 is Unit-LRP results of HAR dataset. (Column 1) Unit 55 is activated by the convex area. Neither LRP score nor uncertainty is not high. (Column 2) Unit 49 is activated by some peaks. Data 986 and 2534 consist of many concave hills, but some peaks are not activated. (Column 3) Similarly, unit 9 is activated by some peak points with uncertainty. (Column 4) Opposite others, unit 31 is activated by the lowest point of each period. As contours are thicker than others, this unit has higher uncertainty than others.

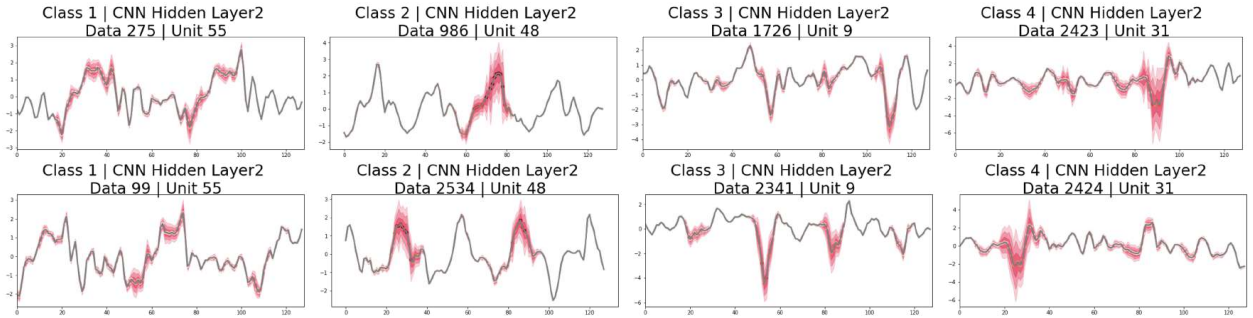


Figure 9: Unit-LRP with uncertainty result from HAR dataset

EEG Dataset

Similar important time points in 10 have a high relevance score from Unit-LRP method as CPHAP method. However, it also shows some important input points before and after the pattern period that CPHAP did not provide.

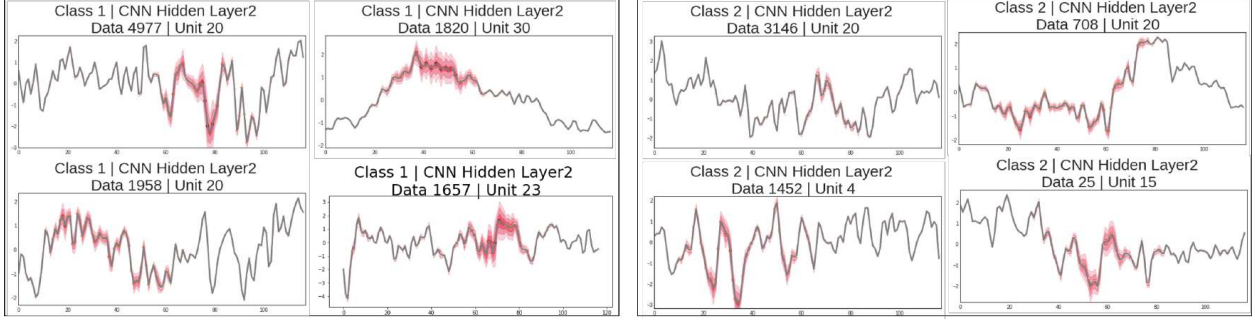


Figure 10: Unit-LRP with uncertainty result from EEG dataset

5.4 Perturbation on critical period

Changing the input sub-sequences, that significantly effects on the activation of the unit, could affect not only on the activation map but also the result of classification. Therefore, we add the Gaussian noises to the most influential input point (top 1 %) that affected the unit’s activation suggested from our proposed methods. To verify whether our algorithm catch the significant input time point well, we compare the result with adding noises at the point of 1% of input randomly. Figure 11 shows the results of applying the perturbation on Uwave dataset. For each step, 1% important time points suggested from CPHAP and unit-LRP methods are perturbed with adding Gaussian distribution noises. Cumulative major input changes in unit-LRP had the greatest impact on the final outcome, followed by CPHAP. In the method of randomly picking a point, the smallest change was seen.

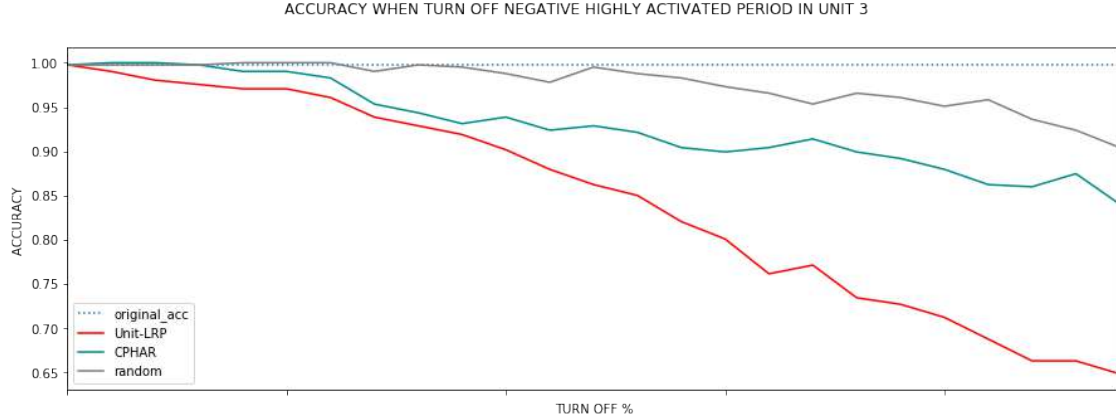


Figure 11: This graph illustrates the results of the positive perturbation on CNN. For each step, 1% time points corresponding to HAP or high LRP scores are perturbed as Gaussian distribution. RAP shows the unique characteristics of the robustness to the perturbation

6 Conclusion

We propose two methods to interpret the decision process of the network by breaking into the activation of units and visualize the relationship between activation of unit and input. We also add uncertainty to this explanation. First, we propose to characterize the receptive field in input from highly active units by two stages of clustering; super-cluster, sub-cluster. Also, we calculate the uncertainty of each cluster which represent coverage of typed important input sub-sequences. Second, we calculate input relevance score to activate unit. Also we obtain uncertainty of these relevance score through perturbations of model. Our proposed methods break down the decision-making process into unit-by-unit roles for easy interpretation, and help people to interpret the temporal neural network intuitively via visualization.

Acknowledgement

This work was supported by IITP grant funded by the Korea government(MSIT) (No.2017-0-01779, XAI)

References

References

- [1] Alexander Binder, Grégoire Montavon, Sebastian Lapuschkin, Klaus-Robert Müller, and Wojciech Samek. Layer-wise relevance propagation for neural networks with local renormalization layers. In *International Conference on Artificial Neural Networks*, pages 63–71. Springer, 2016.
- [2] Gregoire Montavon, Sebastian Lapuschkin, Alexander Binder, Wojciech Samek, and Klaus-Robert Muller. Explaining nonlinear classification decisions with deep taylor decomposition. *Pattern Recognition*, 65:211 – 222, 2017.
- [3] Hongzhi Li, Joseph G Ellis, Lei Zhang, and Shih-Fu Chang. Patternnet: Visual pattern mining with deep neural network. In *Proceedings of the 2018 ACM on International Conference on Multimedia Retrieval*, pages 291–299, 2018.
- [4] Woo-Jeoung Nam, Jaesik Choi, and Seong-Whan Lee. Relative attributing propagation: Interpreting the comparative contributions of individual units in deep neural networks. *arXiv preprint arXiv:1904.00605*, 2019.
- [5] Avanti Shrikumar, Peyton Greenside, and Anshul Kundaje. Learning important features through propagating activation differences. In *Proceedings of the 34th International Conference on Machine Learning-Volume 70*, pages 3145–3153. JMLR. org, 2017.
- [6] Jost Tobias Springenberg, Alexey Dosovitskiy, Thomas Brox, and Martin Riedmiller. Striving for simplicity: The all convolutional net. *arXiv preprint arXiv:1412.6806*, 2014.
- [7] Ramprasaath R Selvaraju, Michael Cogswell, Abhishek Das, Ramakrishna Vedantam, Devi Parikh, and Dhruv Batra. Grad-cam: Visual explanations from deep networks via gradient-based localization. In *Proceedings of the IEEE international conference on computer vision*, pages 618–626, 2017.
- [8] David Bau, Bolei Zhou, Aditya Khosla, Aude Oliva, and Antonio Torralba. Network dissection: Quantifying interpretability of deep visual representations. In *Proceedings of the IEEE conference on computer vision and pattern recognition*, pages 6541–6549, 2017.
- [9] David Bau, Jun-Yan Zhu, Hendrik Strobelt, Bolei Zhou, Joshua B Tenenbaum, William T Freeman, and Antonio Torralba. Gan dissection: Visualizing and understanding generative adversarial networks. *arXiv preprint arXiv:1811.10597*, 2018.
- [10] Edward Choi, Mohammad Taha Bahadori, Jimeng Sun, Joshua Kulas, Andy Schuetz, and Walter Stewart. Retain: An interpretable predictive model for healthcare using reverse time attention mechanism. In *Advances in Neural Information Processing Systems*, pages 3504–3512, 2016.
- [11] Jay Heo, Hae Beom Lee, Saehoon Kim, Juho Lee, Kwang Joon Kim, Eunho Yang, and Sung Ju Hwang. Uncertainty-aware attention for reliable interpretation and prediction. In *Advances in Neural Information Processing Systems*, pages 909–918, 2018.
- [12] Jacob Andreas, Marcus Rohrbach, Trevor Darrell, and Dan Klein. Neural module networks. In *Proceedings of the IEEE Conference on Computer Vision and Pattern Recognition*, pages 39–48, 2016.
- [13] Yann LeCun, Léon Bottou, Yoshua Bengio, and Patrick Haffner. Gradient-based learning applied to document recognition. *Proceedings of the IEEE*, 86(11):2278–2324, 1998.
- [14] Sebastian Bach, Alexander Binder, Gregoire Montavon, Frederick Klauschen, Klaus-Robert Muller, and Wojciech Samek. On pixel-wise explanations for non-linear classifier decisions by layer-wise relevance propagation. *PLOS ONE*, 10:1–46, 07 2015.
- [15] Yarin Gal and Zoubin Ghahramani. Dropout as a bayesian approximation: Representing model uncertainty in deep learning, 2015.
- [16] Jacob Kauffmann, Malte Esders, Grégoire Montavon, Wojciech Samek, and Klaus-Robert Müller. From clustering to cluster explanations via neural networks. *arXiv preprint arXiv:1906.07633*, 2019.
- [17] Sean J Taylor and Benjamin Letham. Forecasting at scale. *The American Statistician*, 72:37–45, 2018.
- [18] John Paparrizos and Luis Gravano. k-shape: Efficient and accurate clustering of time series. *ACM SIGMOD Record*, 45:69–76, 06 2016.
- [19] Jiayang Liu, Lin Zhong, Jehan Wickramasuriya, and Venu Vasudevan. uwave: Accelerometer-based personalized gesture recognition and its applications. *Pervasive and Mobile Computing*, 5(6):657–675, 2009.
- [20] Dheeru Dua and Casey Graff. UCI machine learning repository, 2017.

- [21] Xiao Lei Zhang, Henri Begleiter, Bernice Porjesz, Wenyu Wang, and Ann Litke. Event related potentials during object recognition tasks. *Brain Research Bulletin*, 38(6):531–538, 1995.
- [22] Matthew D Zeiler and Rob Fergus. Visualizing and understanding convolutional networks. In *European conference on computer vision*, pages 818–833. Springer, 2014.
- [23] Giyoung Jeon, Haedong Jeong, and Jaesik Choi. An efficient explorative sampling considering the generative boundaries of deep generative neural networks. *arXiv preprint arXiv:1912.05827*, 2019.
- [24] Rui Zhao, Wanli Ouyang, Hongsheng Li, and Xiaogang Wang. Saliency detection by multi-context deep learning. In *Proceedings of the IEEE Conference on Computer Vision and Pattern Recognition*, pages 1265–1274, 2015.
- [25] Lisa Anne Hendricks, Zeynep Akata, Marcus Rohrbach, Jeff Donahue, Bernt Schiele, and Trevor Darrell. Generating visual explanations. In *European Conference on Computer Vision*, pages 3–19. Springer, 2016.
- [26] Yunseong Hwang, Anh Tong, and Jaesik Choi. Automatic construction of nonparametric relational regression models for multiple time series. In *International Conference on Machine Learning*, pages 3030–3039, 2016.
- [27] Margareta Ackerman, Shai Ben-David, Simina Brânzei, and David Loker. Weighted clustering, 2011.
- [28] Zhiguang Wang, Weizhong Yan, and Tim Oates. Time series classification from scratch with deep neural networks: A strong baseline. In *2017 International joint conference on neural networks (IJCNN)*, pages 1578–1585. IEEE, 2017.
- [29] Asma Ghandeharioun, Brian Eoff, Brendan Jou, and Rosalind W Picard. Characterizing sources of uncertainty to proxy calibration and disambiguate annotator and data bias. *arXiv preprint arXiv:1909.09285*, 2019.
- [30] Hoang Anh Dau, Eamonn Keogh, Kaveh Kamgar, Chin-Chia Michael Yeh, Yan Zhu, Shaghayegh Gharghabi, Chotirat Ann Ratanamahatana, Yanping, Bing Hu, Nurjahan Begum, Anthony Bagnall, Abdullah Mueen, Gustavo Batista, and Hexagon-ML. The ucr time series classification archive, October 2018. https://www.cs.ucr.edu/~eamonn/time_series_data_2018/.

Uwave : Layer 2

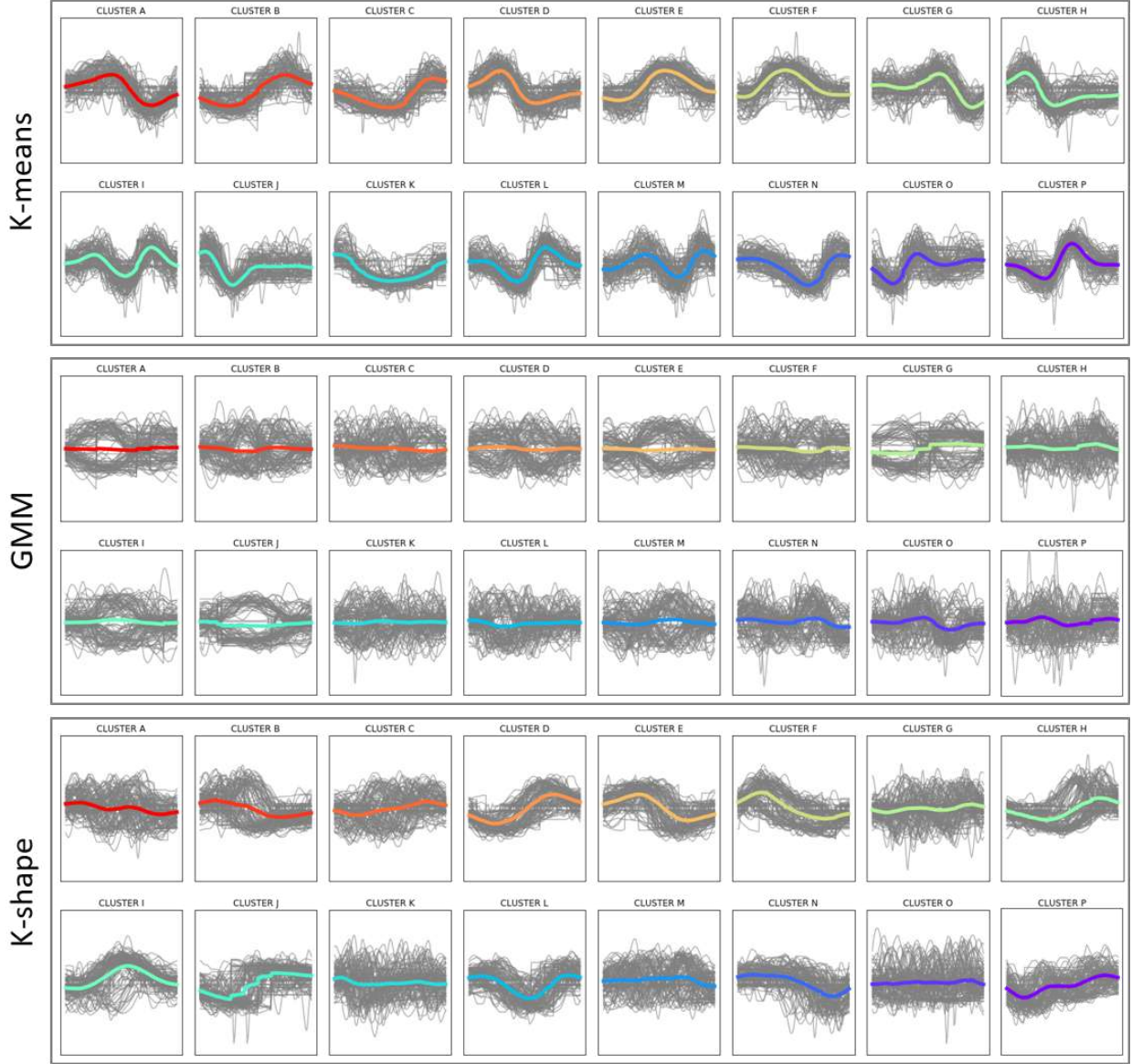


Figure 12: Comparison of various clustering methods for Layer 2 of Uwave dataset

HAR : Layer 2

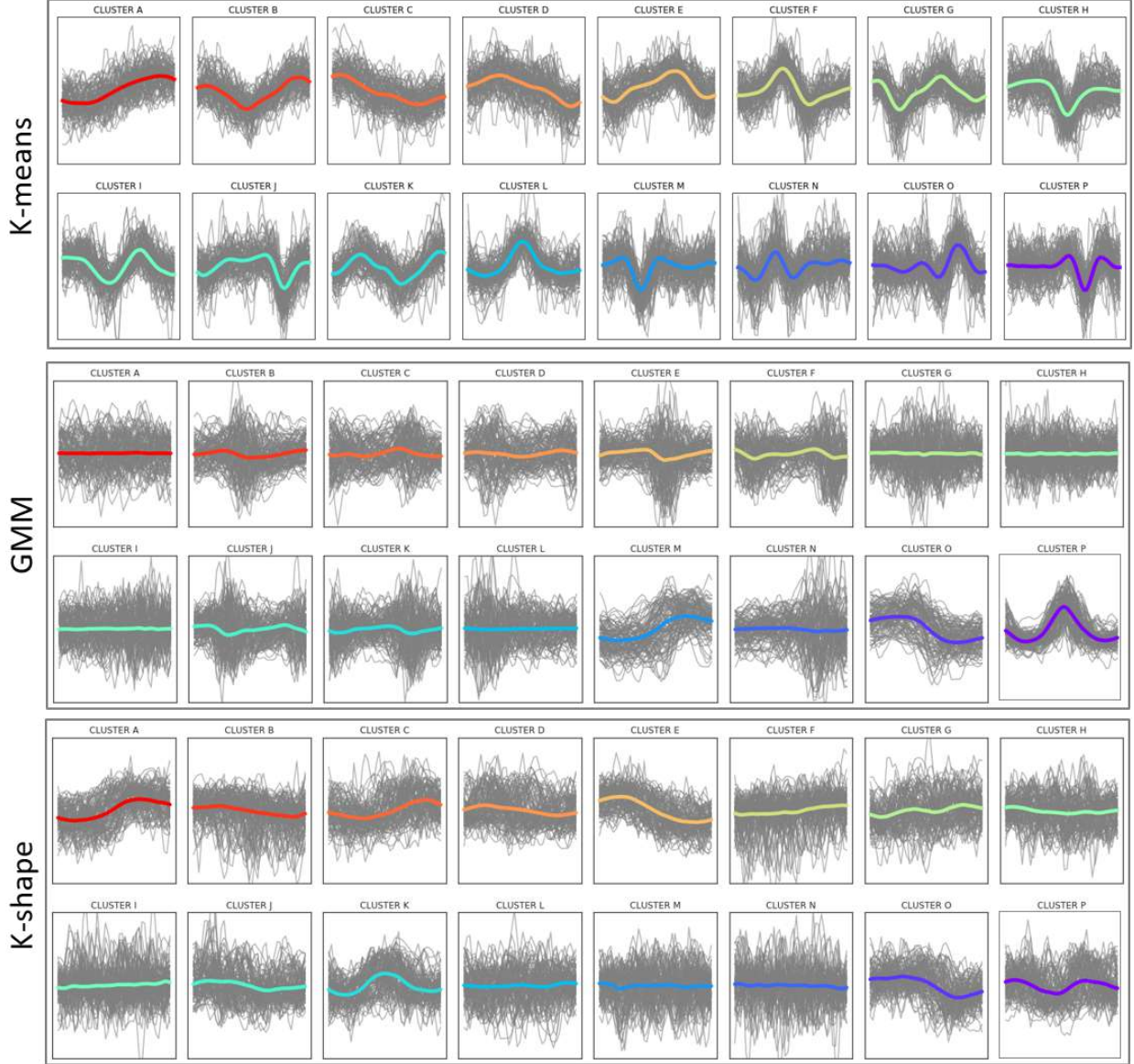


Figure 13: Comparison of various clustering methods for Layer 2 of HAR dataset

EEG : Layer 2

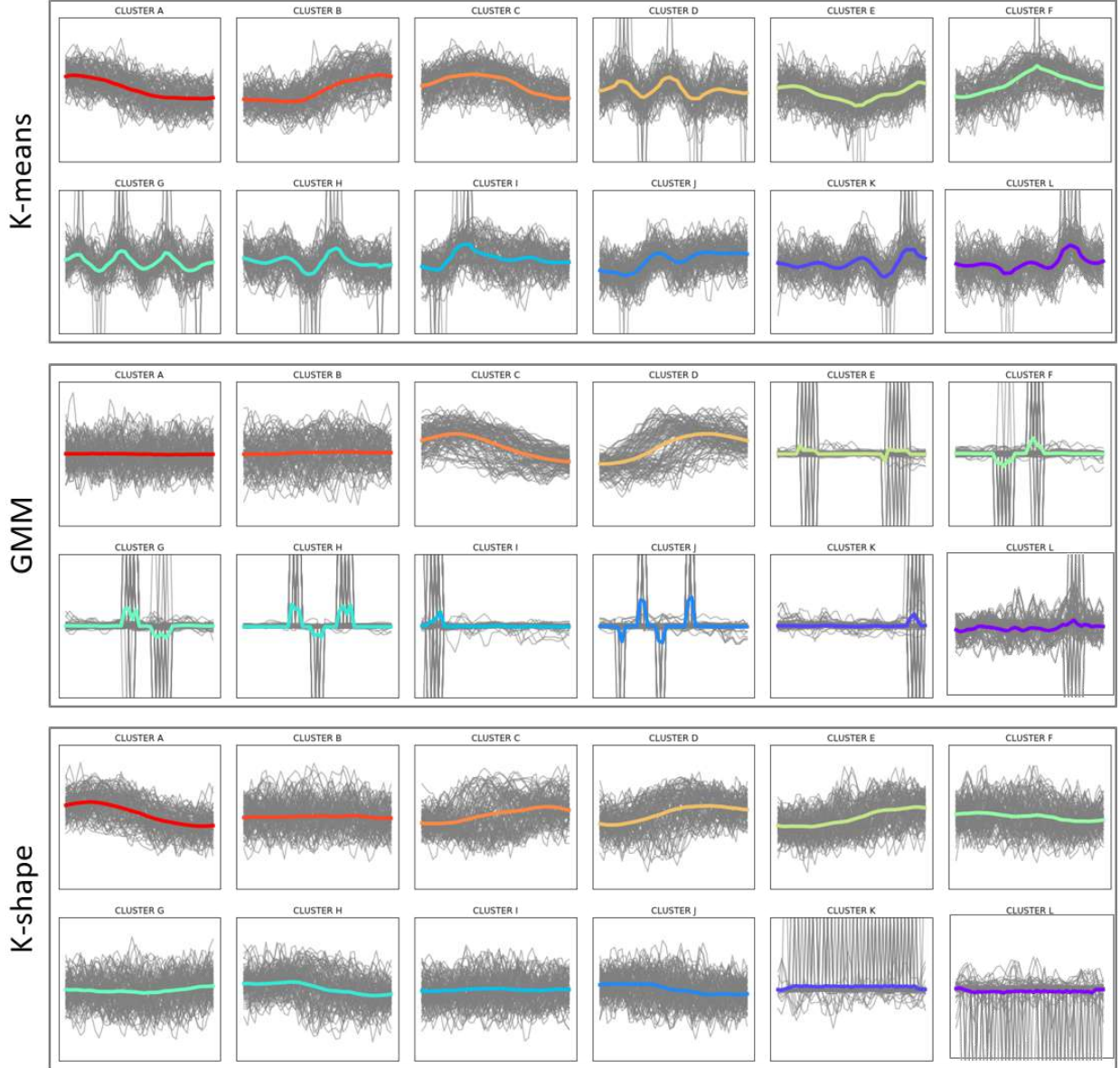


Figure 14: Comparison of various clustering methods for Layer 2 of EEG dataset

Uwave : Layer 2

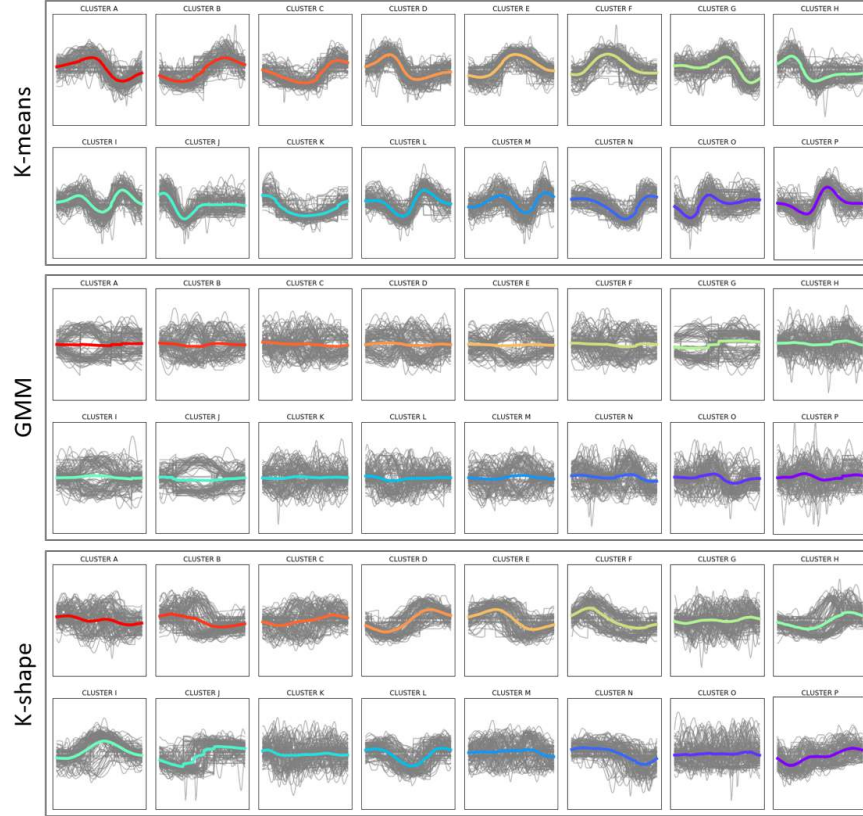


Figure 15: Clustered Patterns with Uwave dataset for Layers 1, 2, and 3. In shallow Layers, simple and short patterns appear, with deeper and longer, complex patterns.

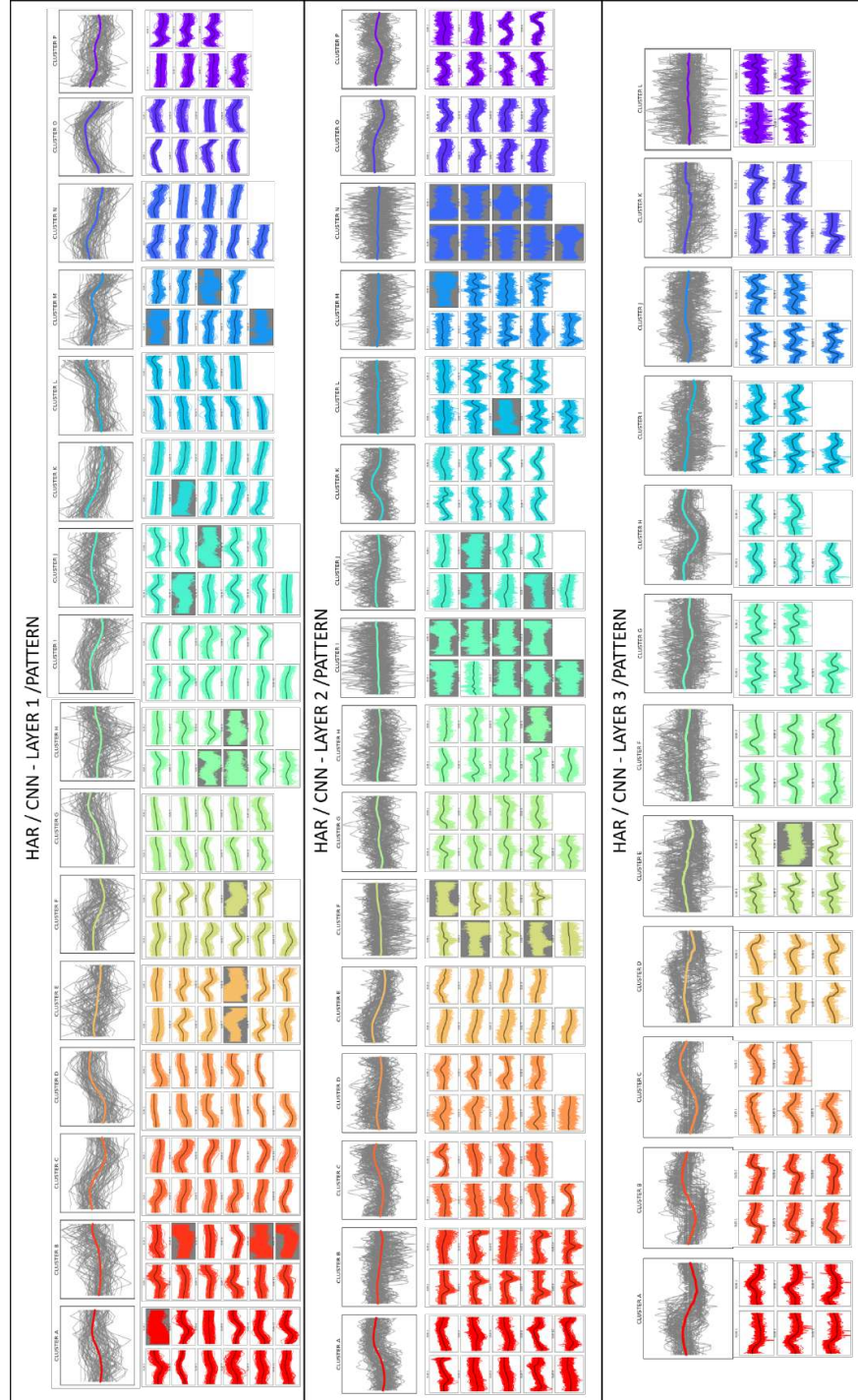


Figure 16: Clustered Patterns with HAR dataset for Layers 1, 2, and 3. In shallow Layers, simple and short patterns appear, with deeper and longer, complex patterns.

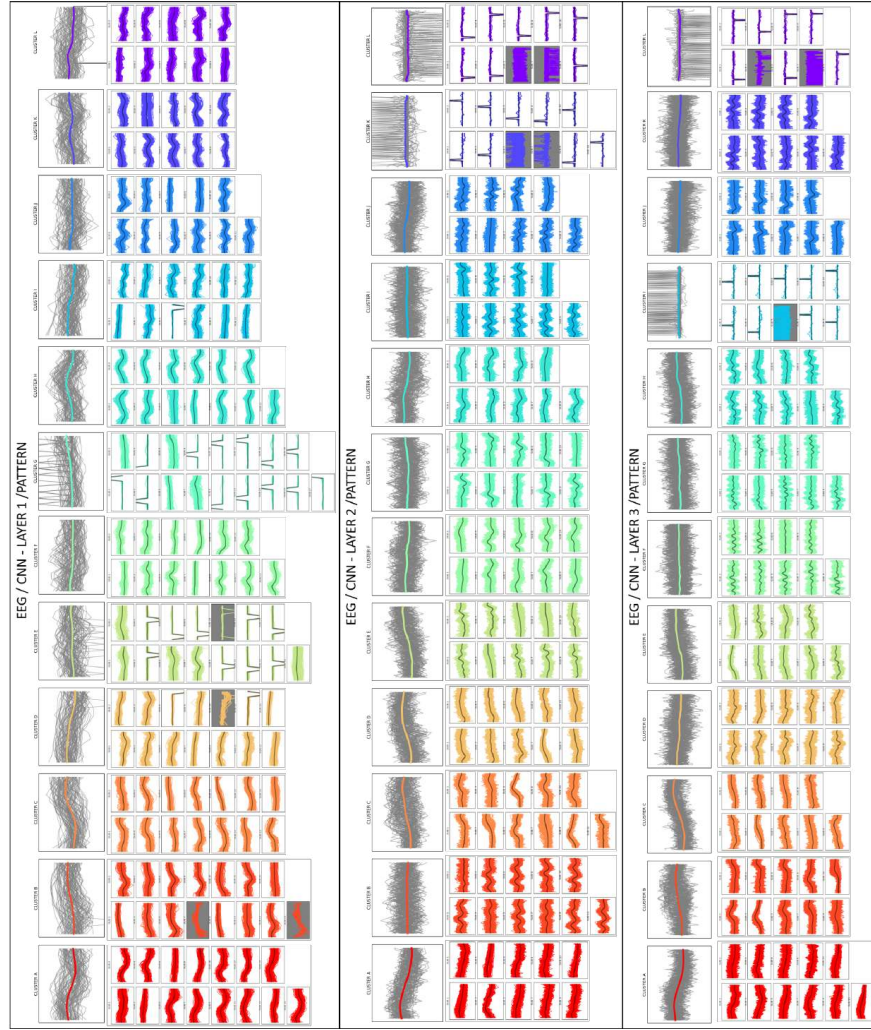


Figure 17: Clustered Patterns with EEG dataset for Layers 1, 2, and 3. In shallow Layers, simple and short patterns appear, with deeper and longer, complex patterns.